JGR Atmospheres

RESEARCH ARTICLE
10.1029/2020JD033170

Optical Spectra of Small-Scale Sprite Features Observed at 10,000 fps

H. C. Stenbaek-Nielsen[1], M. G. McHarg[2], R. Haaland[3], and A. Luque[4]

[1]Geophysical Institute, University of Alaska Fairbanks, Fairbanks, AK, USA, [2]Space Physics and Atmospheric Research Center, U.S. Air Force Academy, Colorado Springs, CO, USA, [3]Arts and Sciences, Augsburg University, Minneapolis, MN, USA, [4]Instituto de Astrofísica de Andalucía (IAA), CSIC, Granada, Spain

Key Points:
- Spectra of small-scale sprite features (downward and upward streamers, beads, and glow) have been recorded at 10,000 spectra per second
- The spectra are dominated by molecular nitrogen emissions; the relative blue and red emission rates can be used to assess the processes leading to the emissions
- Blue emissions are almost exclusively associated with sprite streamers indicating more energetic processes compared to those associated with beads and glow

Correspondence to:
H. C. Stenbaek-Nielsen,
hcnielsen@alaska.edu

Citation:
Stenbaek-Nielsen, H. C., McHarg, M. G., Haaland, R., & Luque, A. (2020). Optical spectra of small-scale sprite features observed at 10,000 fps. *Journal of Geophysical Research: Atmospheres*, *125*, e2020JD033170. https://doi.org/10.1029/2020JD033170

Received 26 MAY 2020
Accepted 25 SEP 2020
Accepted article online 1 OCT 2020

Abstract Spectra of small-scale sprite structures, downward and upward propagating streamers, glow, and beads, were recorded with a slitless spectrograph at 10,000 frames per second (fps) from aircraft missions in 2009 and 2013. The spectra are dominated by emissions from molecular nitrogen, the first positive band in the red, and in the blue the second positive band plus the first negative band of molecular nitrogen ions. The excitation threshold for the blue emissions is higher than for the red emissions, so the blue/red ratio can, in principle, be used as a proxy for the electron energy leading to the emissions. We extracted for analysis time series of spectra from 11 sprites: 18 time series from downward propagating streamers, 6 from upward propagating streamers, 14 from glow, and 12 from beads. The total number of spectra in the 50 time series is 953. Blue emissions are almost exclusively associated with streamers indicating the more energetic nature of streamers compared with glow and beads. Both downward and upward propagating streamers start and end with low blue emissions indicating time variations in the associated processes. Because the red and blue nitrogen emissions are significantly affected by quenching, which is altitude dependent, and we do not have sufficiently accurate altitudes, the observed spectral blue/red ratios cannot be directly applied to sprite models.

1. Introduction

Optical spectra of sprites, first obtained by Mende et al. (1995) and Hampton et al. (1996), are dominated by molecular nitrogen band emissions: the first positive band system (1PN2) in the red and in the blue the second positive band system (2PN2) and the first negative band system of molecular nitrogen ions (1NN2+). The excitation threshold for the first and second positive system is 7.4 and 11.0 eV, respectively, while ionization requires 15.6 eV (Cartwright, 1978; Vallance Jones, 1974). The emissions are very bright, and they are readily identifiable in spectra recorded at 10,000 frames per second (fps) (Kanmae et al., 2010a) and therefore may be used to evaluate the temporal development of the characteristic energy of the electrons leading to the emissions.

The use of spectral features to evaluate the causal processes is not new. Suszcynsky et al. (1998) and Armstrong et al. (2000) compared emissions in the 380–450 nm region (blue) to emissions in the 600–900 nm region (red) and suggested that there are two separate mechanisms associated with the sprite emissions: an initial energetic process followed by less energetic processes. The observations were made from aircraft using photometers together with 30 fps video cameras. Morrill et al. (2002), also using aircraft data, found that emissions in sprite streamers indicate higher electron energies at lower altitudes. Similarly, Kuo et al. (2005), Liu et al. (2006), and Liu, Pasko, Adams, et al. (2009) used data from a spectrophotometer onboard the FORMOSAT-2 satellite to derive the characteristic electron energies and associated ambient electric fields. Pasko (2007, 2010) discussed, based on earlier work by Gallimberti et al. (1974), the use of 1NN2+ and 2PN2 emissions to obtain the electron energy and the driving electric field. More recently, Gordillo-Vázquez et al. (2018) used sprite spectra with 0.24 nm resolution to derive mesospheric temperatures and found no measurable heating of the neutral atmosphere. Finally, modeling by Pérez-Invernón et al. (2018) indicate that the ratio of 1PN2 to 2PN2, the emissions that dominate the 10,000 fps observations presented in this paper, does not vary much for reduced electric fields above ~200 Td but is adequate at lower fields. They suggest that a better ratio might be 1PN2 or 2PN2 to 1NN2+, as suggested earlier by Pasko (2007, 2010).

Sprites develop on millisecond time scales, and they have complex spatial structures with scale sizes down to a few tens of meters. This obviously places severe limitations on observations made with traditional photometers and 30 fps video cameras. Fortunately, sprites are very bright, and therefore most of these limitations were overcome once high-speed imaging became available. Using high-speed imaging, it is possible to observe sprites with sufficient temporal and spatial resolution to document details of sprite morphology (e.g., Cummer et al., 2006; McHarg et al., 2007; Stanley et al., 1999; Stenbaek-Nielsen et al., 2000, 2013; Stenbaek-Nielsen & McHarg, 2008).

Sprite spectra with 3 ms temporal resolution were recorded in 2005 with a slit spectrograph (Kanmae et al., 2007). During the same 2005 campaign images were also recorded at 10,000 fps (0.1 ms temporal resolution). The images showed that sprite streamers are fast moving, small-scale, but very bright features (Stenbaek-Nielsen et al., 2007). This makes them well suited for slitless spectroscopy, and in 2009 sprite spectra using this technique were recorded at 10,000 fps (Kanmae et al., 2010a). While the slitless spectra have less spectral resolution than those recorded with the slit spectrograph, spectra can be recorded within a much larger field of view, and spectra can be obtained of streamers as they propagate across the field of view. This will allow an investigation of temporal changes to the spectra.

Both the 2005 and the 2007 observations were made from the ground. Contrary to expectations, no blue emissions were detected, and it was suggested that the reason was absorption and scattering in the lower atmosphere. The 2009 spectra were recorded from an aircraft at high altitude, and, indeed, emissions in the blue were detected. Evaluating these observations Kanmae et al. (2010b) showed the more energetic nature of streamers compared to the static glows commonly observed in sprites following streamer activity. A second similar aircraft mission was conducted in 2013.

There are many dynamic and bright small-scale features in sprites which are ideally suited for high-speed slitless spectroscopy, and in this paper we present an analysis of spectra obtained at 10,000 fps in the 2009 and 2013 aircraft sprite missions. We evaluate nitrogen emissions in the blue and red from four sprite features: downward and upward propagating streamers, sprite glow, and beads. Streamers are mainly observed in the initial phase of a sprite event, while glow and beads are longer lasting and largely stationary. Glow and beads are typically the main sprite features in video recordings (30 or 25 fps).

The spectra are dominated by molecular nitrogen emissions. Most of the spectra have a well-defined spectral signature between 625 and 700 nm in the red. This is the $\Delta\nu = 3$ bands in the first positive system of molecular nitrogen. While they are generally less bright than the $\Delta\nu = 2$ bands in the 720–780 nm range, they are better defined in our data, and we use them as primary selection criterion when selecting events. The wavelength range used for the blue emissions is 380–450 nm, which covers part of the 2P system of molecular nitrogen and molecular nitrogen ions. The 380 nm limit is the spectrograph low wavelength cutoff, and therefore only the longer wavelength bands of the 2P system will be detected. The spectrograph does not have enough resolution to fully separate 2PN2 and molecular nitrogen ion emissions, but since both require higher energies to emit than the 1PN2 band, alone the presence of blue in the spectra will indicate a more energetic process.

The nitrogen emissions are affected by quenching deactivation of the excited molecules by atmospheric collisions, rather than through photon emissions, which becomes important at lower altitudes where the radiative life time, 6 μs for 1PN2 and 50 ns for 1PN2, becomes longer than the time between collisions with atmospheric molecules. Hence, if the observed emissions are to be used with models to infer the characteristic electron energies involved, which would be an obvious next step, the emissions have to be corrected for quenching. Unfortunately, there is a substantial uncertainty on the altitudes of the emitting sprite features, which, in effect, prevents the observations to be used quantitatively with models. We discuss this in detail in sections 4.1 and 4.2 below. Nevertheless, the ratio of blue to red emissions derived from our observed spectra is a convenient parameter for an evaluation of systematic differences between the four small-scale sprite features. In section 4.3 we present ratio averages across the entire data set, and in section 4.4 temporal changes observed within individual spectral time series.

2. Instrumentation

Essentially the same slitless spectrograph was used in the 2009 and 2013 recordings at 10,000 fps. It was configured with a 100 lines/mm transmission grating blazed at 425 nm in front of a Nikon 50 mm f/1.4 lens on a Video Scope VS4-1845HS image intensifier. The extended blue response intensifier has a P24 phosphor

(10 μs decay) preventing persistence onto following images. The intensified spectral image is relayed to the Complementary Metal Oxide Semiconductor (CMOS) chip of a Vision Research Phantom high-speed camera. The Phantom camera uses GPS time, and it is configured and controlled by a laptop computer which is also used for the storage of events initially recorded in camera memory.

In 2009 we used a Phantom v7.1, which has 12 bit images, and in 2013 an improved Phantom v7.3 with 14 bit images. Both models use the same 800 × 600 pixel format CMOS chip, but at 10,000 fps hardware limitations reduce the usable image size. For the v7.1 (2009) we configured the Phantoms to 640 × 256 and for the v7.3 (2013) to 640 × 320 pixel image formats, corresponding to a field of view of 15 × 6° and 15 × 7.5°, respectively.

The spectrograph was mounted on an adjustable azimuth-elevation mount looking out through one of the left side windows on the aircraft. Comounted with the spectrograph we had a low-light-level video camera (Watec 902H) to provide scene awareness and to record star background critical for accurate pointing information. On a separate mount, looking through another window, we had a second Phantom camera configured as an imager and a comounted Watec video camera, but these data were not used directly in the analysis presented here.

The spectrograph was wavelength calibrated using an Ocean Optics HG-1 Mercury Argon Calibration Source. The dispersion is 4.05 nm/pixel, and it varies only slightly across the field of view. During the missions we recorded spectra of a number of bright stars with known spectra. Analysis of the 2009 spectra, corrected for atmospheric transmittance, shows a response across the visible and near-IR from 380 to 900 nm with a steep falloff in the blue and a peak response around 550 nm (Kanmae et al., 2010b). Normalized to the maximum at 550 nm, the response in the red is 0.87 at 625 nm and 0.65 at 700 nm. The 625–700 nm is the wavelength window used in the analysis presented in this paper. In the blue wavelength section the response is 0.78 at 450 nm falling off to 0.05 at 380 nm.

In the 2013 mission we looked through a quartz window expecting better response in the blue, but that was not the case, and we found the blue cutoff is primarily due to the transmission characteristics of the Nikon 50 mm lens. While the blue response in the 2013 mission was slightly better we did not find in the analysis any material differences between the spectra from the 2009 and the 2013 missions.

Most of the molecular nitrogen 2P bands emits at shorter wavelengths than the 380 nm instrument cutoff, which is unfortunate. On the other hand, the 2P bands are bright, and the cutoff prevents second-order spectra to interfere with the first-order spectra which simplifies analysis considerably.

Getting the spectral information with slitless spectroscopy requires small sources, ideally, as in astronomy, point sources. In that case the resolution would be 4.05 nm/pixel. While the sprite structures analyzed here are small, they are not point sources but extended sources resulting in lower spectral resolution. Also, many features, especially streamers, vary in brightness. As the brightness changes the size in the images typically changes and with it the spectral resolution. The structures analyzed are typically 3 to 10 pixels wide, and the resolution would then be ~15–40 nm. This is not sufficient for a clear separation of the neutral and ion emissions in the blue but acceptable when we just want to isolate the signals in the wavelength regions of the 1PN2 and 2PN2 bands.

With the 100 lines/mm grating first-order spectra covering 0 to 800 nm are ~200 pixels wide, which is approximately one third of the 640 pixel image width. On one of the flights in 2009 we used a 200 lines/mm grating to provide twice the spectral resolution, but the wider spectra (in pixels) significantly reduces the area in the image from which spectra can be recorded, and it resulted in an unacceptable loss of otherwise usable events.

3. Data

Sprites and their spectra were recorded at 10,000 fps in the 2009 and 2013 aircraft missions over the U.S. Midwest region. Additionally, we recorded GPS aircraft position with 1 s temporal resolution and lightning strikes from the National Lightning Detection Network (NLDN). A total of 60 sprites with spectra were recorded, but because of overlap of spectral features within an image, only relatively few events will produce spectra where the 1P (red) and 2P (blue) bands from particular sprite features are sufficiently isolated to allow evaluation. Only 2 of the 60 events were found to have all four sprite features, downward and upward propagating streamers, beads, and glow, present with spectra of sufficient quality for evaluation. However,

there were a number of events with good spectra for two and three features thus allowing for a more statistical analysis.

For analysis we selected 11 events. An event was selected if it has usable spectra for at least two of the four sprite features in the analysis. The $\Delta\nu = 3$ band of the 1P system of molecular nitrogen is typically a well-defined feature in the spectra. It is observed between 625 and 700 nm, and we used that spectral feature as primary selection criteria. For each feature within an event we then extracted as many sequential spectra as possible to provide data for an evaluation of the temporal development of the blue and red emissions. The 11 events yielded 50 sequences of spectra, 18 of downward streamers, 6 of upward streamers, 14 of glows, and 12 of beads. The total number of spectra in the 50 sprite feature sequences is 953.

Most of the spectra were present against a dark background, but there were some where otherwise well-defined spectral features were observed against a relatively uniform background created, for example, by the presence of a sprite halo. In this case we used background subtraction to isolate the spectral features of interest.

For comparison with models of the processes leading to the emissions, the observed ratios should be corrected for atmospheric transmission losses and for instrument response. The atmospheric transmission losses and the instrument response have been presented by Kanmae et al. (2010b), and the instrument response function was briefly described in the previous section. The atmospheric transmittance was calculated for the altitude and typical elevation angles of the observations using the Moderate Spectral Atmospheric Radiance and Transfer (MOSART) code (Cornette et al., 1995). In the blue wavelength range, 380–450 nm, the transmittance is 0.62–0.76, and in the red wavelength range, 625–700 nm, it is 0.76–0.90.

The N_2 emissions in the 380–450 nm wavelength window are from 2PN2 and 1NN2+. The ion emission at 427.8 nm is often used to identify N_2^+ as there are no serious competing emissions nearby, but going through the data set reported here, we found no spectral time series where the 427.8 nm emission was sufficiently distinct for more detailed analysis. Effectively, we do not have enough spectral resolution to separate the ion and neutral emissions. There is also a higher uncertainty on the instrument response near the 380 nm cutoff, which combined with the steep falloff in the response near the cutoff may introduce significant errors in the derived blue signal. Therefore, we decided not to correct for transmission losses and instrument response.

The spectra are affected by atmospheric turbulence and by noise originating primarily in the camera intensifier. To evaluate this, we analyzed spectra from the planet Jupiter which was in the field of view in a sprite recorded on 27 August 2009 at 09:15:23 UT. We extracted 200 consecutive spectra, 0.02 s of data, and assuming that the emissions from Jupiter do not vary over the 0.02 s data sequence, the scatter in the brightness, which appears to be random, will reflect the uncertainty thus introduced on the data. To be consistent with the analysis presented in this paper, we evaluated the scatter for the same spectral bands, 380–450 nm in the blue and 625–700 nm in the red, used for the data analysis presented in this paper. Details of the procedure are given in section 4 below. The standard deviation in the red is 793 on a ~10,000 signal (8%) and for the blue 856 on a ~5,000 signal (19%). Following standard error analysis procedures (Taylor, 1997), we will use the Jupiter data to estimate error bars on temporal variations in spectra from individual sprites presented in section 4.4 below.

4. Analysis

Figure 1 shows an example of each of the analyzed features: downward and upward propagating streamers, glow, and bead. Each of the four sections in the figure has to the left a 281 × 256 pixel (6.7 × 6.1° field of view) subimage extracted from the original image, and to the right the derived spectrum. The location of the sprite feature (the zero-order spectrum) is given by the white vertical lines at top and bottom of each image. The feature and associated spectrum is bracketed by two white dashed horizontal lines which define the section of the columns over which we integrated to get the spectral signal. The number of pixels in the section, typically between 3 and 6, was set individually for each sequence to optimize the quality of the derived spectra. (The horizontal lines also have a small slant to compensate for the grating not being exactly aligned with the rows in the spectrograph Charge-Coupled Device (CCD). The first-order spectrum is seen toward the right in the subimage. The second-order spectrum would be located farther to the right and outside the subimage but is rarely detected. In the panel to the right of the image we show the spectrum derived by summing image

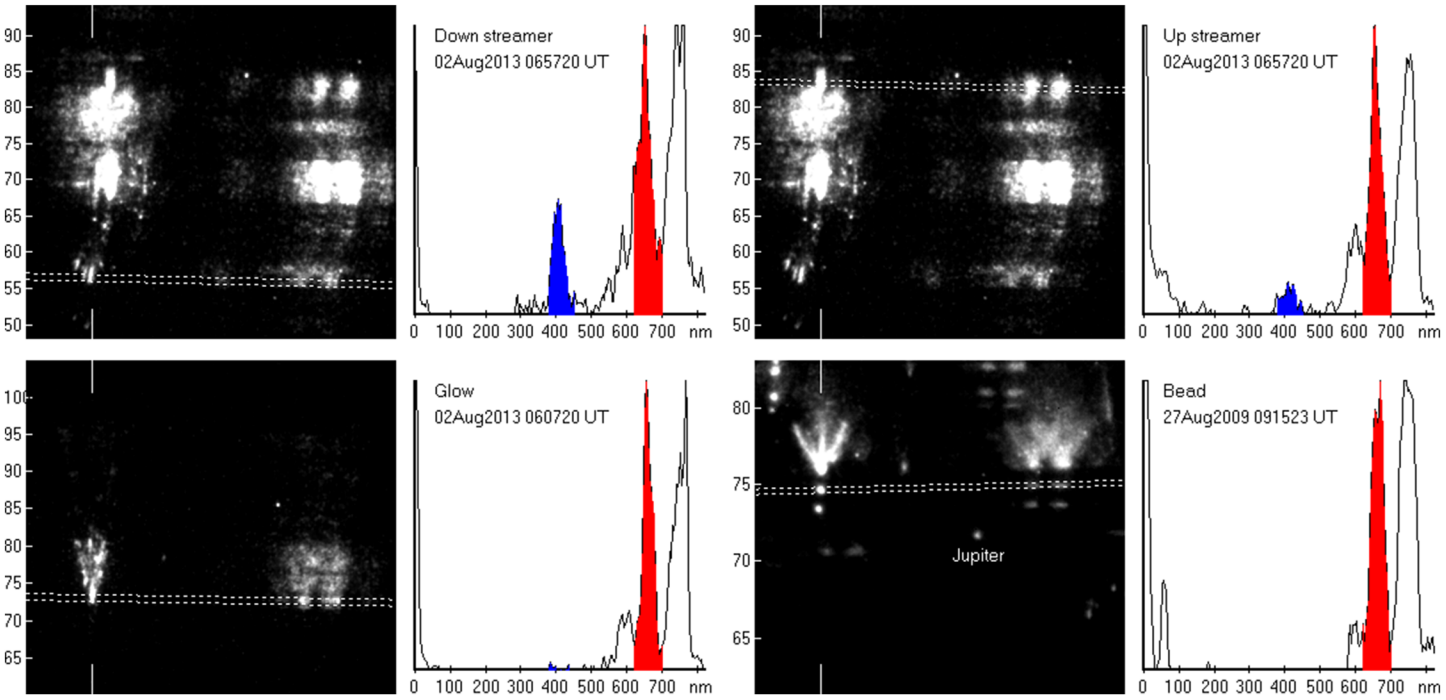

Figure 1. Examples of spectra: Downward and upward propagating streamers, glow, and bead. Note the example of downward and upward propagating streamers are from the same event. The spectra are normalized to the $\Delta\nu = 3$ band of the 1P system in the red to allow easy visual comparison with the more energetic 2P system and the 1NN2+ emissions in the blue. Note Jupiter in the field of view of the sprite in the lower right panel.

pixel values in each image column between the two horizontal lines. The spectrum is wavelength scaled using 4.05 nm/pixel, as derived from a wavelength calibration, and the location of the zero-order spectrum as origin. To allow easy visual comparison between individual spectra within a sequence and between sequences, we scaled all spectra to a fixed amplitude of the $\Delta\nu = 3$ bands of the 1P system of molecular nitrogen. The blue section covers the wavelength range 380–450 nm and is shown in blue. The red section, 625–700 nm, is shown in red.

In the four examples presented in Figure 1 we note that blue emissions, indicating a more energetic process, are only prominent in streamer spectra (upper row of Figure 1). This is generally true for the entire data set analyzed. The downward and upward streamer examples in Figure 1 are from the same event (same image used in the figure). However, when comparing the two spectra, or any set of spectra from other events, quenching, which is altitude dependent, must be considered.

4.1. Uncertainty on Altitude

The altitude of the emitting sprite feature is typically calculated from the elevation angle of the feature together with the range to the sprite. The high-speed camera had a coaligned low-light-level video camera which provides good star fields from which the elevation angle to the sprite feature can be accurately determined, and the range is given by assuming that the sprite is at the same distance from the aircraft as the causal lightning strike recorded by NLDN.

The assumption of the sprite located at the same range as the lightning strike is very common and often, by necessity, made when observations are only available from a single site, as is the case here. However, this may lead to significant errors. We know that sprites can be many tens of km from the lightning strike. Often, as in multiple C-sprite events, many sprites appear across the camera field of view clearly indicating onset of individual sprites across a large area. Lyons (1996) reported sprite locations up to 111 km from the strike; to our knowledge, this is the largest strike to sprite distance reported. Wescott et al. (2001) presented an example where the sprite halo was centered essentially over the lightning location, but the sprites occurred ~20 km from the strike; other triangulated sprite locations in that study were up to 50 km from the associated strike. Sao Sabbas et al. (2003) compared 40 triangulated sprite locations to their causal

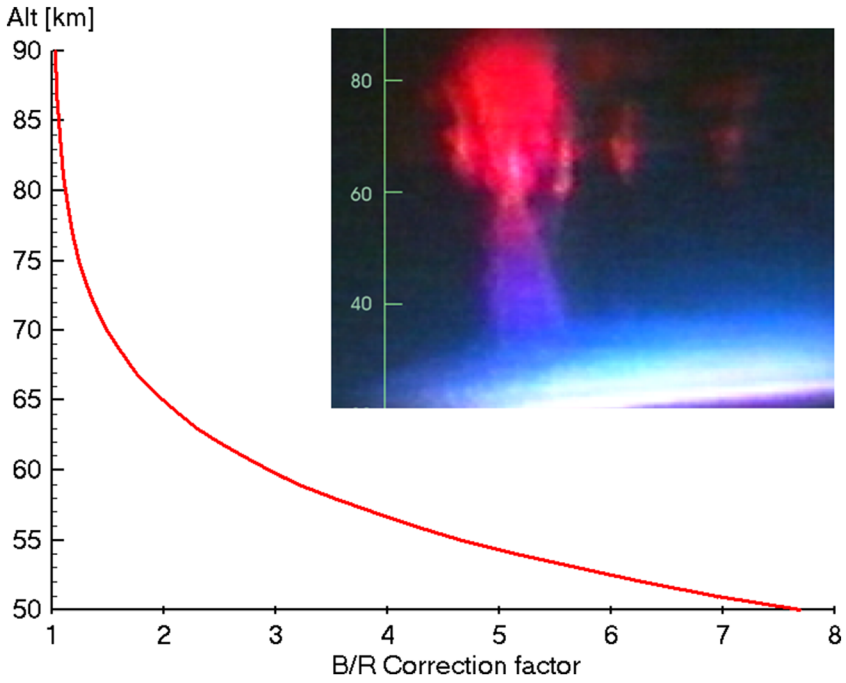

Figure 2. Quenching factor of the blue/red, 2PN2/1PN2, emission ratio based on the MSIS-E-90 model atmosphere with emission and quenching rates from Ihaddadene and Celestin (2017). The inserted color image is from Sentman et al. (1995) recorded with a University of Alaska color TV camera illustrating the effect of quenching. Above 60 km the sprite emisions are dominated by the red 1PN2 emissions, but below 60 km the color gradually changes to blue mainly due to the increasing quenching of the red 1PN2 emissions.

lightning strike and found a mean distance of 40 km; the maximum distance was 82 km. Yang et al. (2015) reported on a sprite more than 38 km from the strike, and Sato et al. (2016) reported sprites 8–20 km from the strikes based on observations from the International Space Station.

Most of the sprites in the data set analyzed here were observed at elevation angles between 10° and 20°, and a change of 40 km in range, the mean distance between strike and sprite reported by Sao Sabbas et al. (2003), at an elevation angle of 15° would change the altitude by 12 km. This is more than one atmospheric scale height which would significantly affect quenching.

4.2. Effect of Quenching

Excited nitrogen molecules, neutrals, and ions, may be deactivated (quenched) by atmospheric collisions before they emit. This process becomes increasingly important at lower altitudes. Armstrong et al. (1998), their Figure 9, shows graphically the altitude effect of quenching on the photon yield: 1PN2 has a yield of 80% at 80 km decreasing to 20% at 60 km; 2PN2 is 80% at 45 km and 20% at 25 km; 1NN2+ is 80% at 60 km decreasing to 20% at 40 km. Thus at sprite altitudes, 60–90 km, the main impact comes from quenching of the 1PN2 band system emitting in the red. All other being equal, the blue emissions should become increasingly prominent with lower altitude.

The altitude dependent increase in the observed blue/red (2PN2/1PN2) ratio due to quenching is shown in Figure 2. The quenching ratio has been calculated using the MSIS-E-90 model atmosphere with newer quenching coefficients given by Ihaddadene and Celestin (2017). A commonly used parameter to describe the effect of quenching is "quenching altitude". This is the altitude where the probability of photon emission and quenching is the same, 50%. For the model used we find the quenching altitude for the 1PN2 and 2PN2 emissions to be 65 and 30 km, respectively. We note that a commonly used reference source, Vallance Jones (1974), gives the two quenching altitudes as 53 and 30 km respectively. The lower quenching altitude given by Vallance Jones appears to come mainly from his assumption of the same quenching rate for O_2 and N_2. The quenching altitude for the 1NN2+ emissions is given by Vallance Jones as 48 km; using newer quenching rates given by Dilecce et al. (2010) we find a quenching altitude of 52 km.

Table 1
Summary of Data Set

	Downward streamer	Upward streamer	Glow	Bead
Number of time series	18	6	12	14
Number of spectra in each	4–21	3–11	5–70	4–77
Observed B/R ratio range	0.058–0.300	0.018–0.164	0.004–0.114	0.000–0.053
Average observed B/R ratio	0.178	0.077	0.034	0.013
Corrected B/R ratio range	0.010–0.179	0.013–0.092	0.003–0.051	0.000–0.020
Average corrected B/R ratio	0.055	0.047	0.017	0.006
Median corrected B/R ratio	0.050	0.057	0.013	0.006

Note. Line 1 = number of time series in each of the four sprite features. Line 2 = range of the number of spectra in each sequence, for example, the number of spectra in the 18 downward streamer sequences vary from 4 to 21. Line 3 = range of averaged ratios within each of the four sprite features. Line 4 = average of the entries in Line 3. Line 5 has the quenching corrected ratio ranges, and Line 6 the corresponding averages. Last line, Line 7, has the median of the quenching corrected averages.

The effect on optical sprite observations is clearly illustrated in the image inserted in Figure 2. The image is from the first color video recording obtained by a University of Alaska TV camera built for auroral research (Sentman et al., 1995). While the top of the sprite is red, the color changes to blue as the red 1PN2 emissions are quenched at lower altitudes. Also contributing to the lower altitude blue emissions are nitrogen ion emissions created in the downward propagating streamer heads.

4.3. Blue and Red Emissions

The examples of the four sprite features (downward and upward propagating streamers, glow, and beads) shown in Figure 1 show that blue emissions, indicating a more energetic process, are mainly prominent in streamers. This is generally true for the entire data set analyzed. To analyze the differences more quantitatively, we extracted from each spectrum the ratio between the blue emissions (380–450 nm) and red emissions (625–700 nm). Then to establish a characteristic B/R ratio for each of the 50 time series we averaged the ratios within each time series. Then we averaged the averages within each of the four sprite features, downward and upward propagating streamers, glows, and beads. Because of the uncertainty on the quenching correction introduced by the assumption of the sprite features located at the same range as the causal lightning strike, we give the statistics for both the observed B/R ratios and the quenching corrected values. The ratios are not corrected for instrument response or atmospheric effects. A summary of the data is given in Table 1.

The summary confirms that the blue emissions are primarily associated with streamers. The average quenching corrected B/R ratios for downward propagating streamers, assumed to be positive streamers, is larger than the ratio for upward propagating streamers, assumed to be negative streamer, as would be expected from models (e.g., Babaeva & Naidis, 1997; Liu & Pasko, 2004; Luque et al., 2008; Qin & Pasko, 2014). However, the observed difference is small and well within the uncertainty on the analysis.

The blue emissions in the 380–450 nm wavelength section have contributions from molecular nitrogen neutrals and ions. About 14% of the entire 2PN2 emissions (estimated from the spectra by Gordillo-Vázquez et al., 2012) and 90% of the 1NN2+ band emissions (estimated from emission rates by Vallance Jones, 1974) are in the 380–450 nm range. The relative contribution from the neutral and ion emissions to the 380–450 nm blue signal depends on the electric field energizing the electrons leading to the emissions. Calculating 1NN2+ emissions relative to the 2PN2 emissions shows that for low fields, $E/n < 200$ Td, emissions in the blue are mostly 2PN2, whereas at higher fields expected associated with streamers, $E/n \sim 800$ Td, about half of the detected blue emissions would be from 1NN2+. The contribution of 1NN2+ emissions to the blue signal will not significantly affect the quenching correction (Figure 2) since, for 60–90 km altitude range, the correction is primarily due to quenching of the red 1PN2 emissions. We do not have sufficient spectral resolution to separate the neutral and ion emissions, but since both the blue neutral and ion emissions require more energetic electrons than the red emissions, the presence of blue emissions will indicate more energetic electrons.

In contrast, the B/R ratios for glow and beads are low. In several of the bead time series analyzed there were no blue emissions detected. Also, in contrast to the streamers, glow and beads are essentially stationary and longer lasting, and consequently, their time series are generally significantly longer.

The largest quenching correction to the observed B/R ratios is for downward streamers. This is not surprising since downward streamers generally propagate to altitudes lower than upward streamers, glow, and beads. With the quenching correction we find the average ratio of downward streamers slightly larger than that of upward streamers in qualitative agreement with streamer models. We tried different assumptions for deriving the altitudes to see the impact on the quenching corrected emission ratios. Pasko and Stenbaek-Nielsen (2002) suggested that the change to very diffuse emissions often seen in the top of carrot sprites around 80 km altitude is associated with a sharp increase in conductivity at the edge of the ionosphere. This morphological boundary is very easy to identify when present. Another method is to set the altitude for a given sprite feature and then adjust the range accordingly. The different assumptions significantly affects the ratios in individual spectral time series, but surprisingly, the average quenching corrected B/R ratio for downward streamers remains slightly higher than that for the upward streamers. Nevertheless, the uncertainty on the ratios remains substantial.

4.4. Temporal Variations in Blue and Red Emissions

The statistical analysis presented in the previous section showed the more energetic nature of streamers relative to glow and beads. We now turn to an evaluation of individual spectral time series to extract information about general systematic temporal changes in the spectra from each of the four small-scale sprite features considered.

Temporal changes in the blue to red ratio may indicate a change in the electron energies leading to the emissions. But a ratio change can also have other reasons. A change in altitude, as observed primarily in streamers, will change the quenching correction of the ratio. The altitude dependent quenching correction factor (Figure 2) is mainly due to quenching of the red 1PN2 emissions, which, in turn, reflects the atmospheric number density. With a constant mesospheric scale height the quenching correction will remove ratio changes within individual time series solely due to altitude changes. The altitude could also be changed by assuming a different range to the event which would increase or decrease all ratios in the time series. In both cases any peaks in the observed ratios would be preserved. Of more concern are temporal changes in the observed spectra due to atmospheric effects and noise in the camera intensifier. A quantitative estimate of this uncertainty was derived, as described in section 3, from spectra of Jupiter, and we will apply this uncertainty to the time series to help validate any temporal variations present in the time series.

The sprite shown in the lower right panel of Figure 1 provided spectral time series for a downward streamer, glow, and two beads, and we show data from this event in Figure 3. The sprite has been discussed earlier by Kanmae et al. (2010b) and by Stenbaek-Nielsen et al. (2013). It is a small and not very bright carrot recorded on 27 August 2009 at 09:15:23 UT over Oklahoma in the U.S. Midwest. It is also the event with Jupiter in the field of view which we use to estimate error bars on the spectral ratios derived.

The top panel of Figure 3 has a series of 50 tall and narrow image strips, 5 ms of time, extracted from the original images to illustrate the morphology. The image used in Figure 1 is at 4.2 ms in Figure 3. The altitude scale, in km, is on the left, and the elevation angle scale, in degrees, on the right. Luminosity from the causal lightning strike was observed 1.0 ms (10 frames) before the start of the strip image time series plot, and we use that for timing. An elve propagated down across the field of view following the lightning strike, and a sprite halo appeared in the high-speed images 0.3 ms after the lightning strike. The panel starts with the first indication of a local intensification within the halo eventually leading to streamer formation at 2.0 ms.

The sprite has usable spectra for the downward propagating streamer dominating the left part of the panel, the associated glow in the top half of the panel, and the two well-defined beads below the glow. The assumed altitudes of the spectra of the streamer and glow are shown in the middle panel, and the quenching corrected blue/red ratios are shown in the bottom panel. We have not plotted data points for the beads since their altitudes do not vary and essentially no blue emissions are present in the bead spectra.

At start of the image time series an intensification in the halo is seen moving slowly down at 0.3×10^7 m/s leading to streamer initiation around 2.1 ms. The spectra for the intensification are very noisy, but there are no obvious blue emissions attributable to the intensification. At the start of the downward propagating streamer blue emissions appear and there is a rapid increase in both streamer brightness and in the blue/red ratio consistent with modeling by Liu, Pasko, Frey, et al. (2009). The maximum streamer brightness is near 2.5 ms at which time a split is observed. The downward velocity of the streamer is initially 1.7 10^7 m/s but starts to

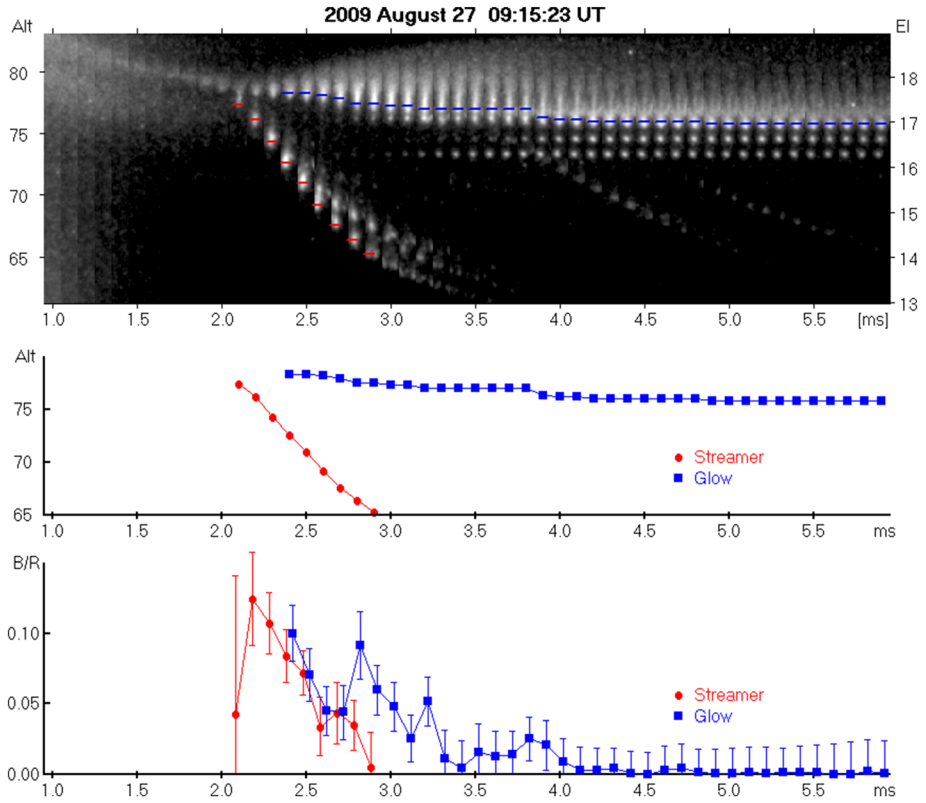

Figure 3. Sprite observed 27 August 2009 at 09:15:23 UT over Oklahoma. The top panel has an image time series starting with the first indication of an intensification leading to streamer formation. The image time series has several streamers, glow, and beads. Spectra of the dominant streamer and the glow above were extracted from a narrow altitude range at the location indicated by the blue and red bars. The middle panel shows the altitudes of the streamer (in red) and the glow (in blue). The bottom panel has the quenching corrected blue to red emission ratios derived from the observed spectra with associated error bars. The time axis is ms from the lightning/elve associated with the sprite. The data points for the streamer and glow ratios have been slightly offset to avoid overlapping error bars.

decrease shortly after the split. The blue/red ratio also decreases rapidly as the streamer propagates down. The end of usable streamer spectra is at 2.9 ms, but the streamer is clearly visible beyond that time. It slows down and fades near the bottom of the field of view.

Bright, stationary glow and beads form after streamer onset near the altitude of the onset. In the strip image time series the glow appears as a continuation of the intensification in the halo leading to the streamer initiation. The glow spectra plotted start two frames from the streamer onset and the entire glow spectral time series has 80 data points. This is 4.5 ms beyond the time covered in Figure 3. The glow expands both up and down and the spectra are from the lower tip of the glow which is the best defined small feature in the glow. There is a faint bead early in the time series at an altitude of 76 km; it brightens as the glow expands down over the bead, and at 3.8 ms the position of the location, where we extract the spectra, is moved down to the bottom of the bead. We see glow extending down over a bead below quite often in our high-speed sprite recordings although in this case the bead remains distinct to the end of the time series.

The blue/red ratio for the glow is initially similar to that of the streamer, and it decreases as the streamer fades. There is a slight increase in the ratio starting around 3.5 ms, which is likely associated with additional streamer activity. For most of the glow, from 3.0 ms until the end of the time series at 9.3 ms, very little blue is detected. This is quite representative of our data; when blue emissions are present, they often appear to be associated with streamer activity early in the sprite event.

Below the glow there are two well-defined beads which formed in the streamer channel some tenths of milliseconds after the streamer passage. This is very typical of sprite bead formation (Luque et al., 2016;

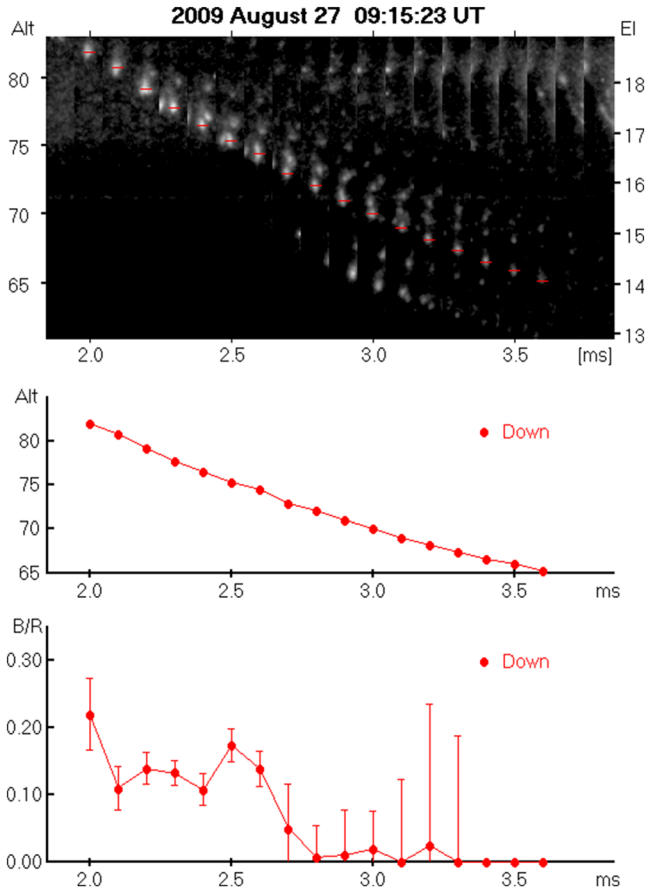

Figure 4. Sprite observed 27 August 2009 at 09:15:23 UT over Oklahoma (from the same event as shown in Figure 3). The top panel has an image time series starting at the time the streamer comes into view with the location of the spectra indicated by a red line segment. The middle panel shows the altitude of the streamer, and the bottom panel has the corresponding quenching corrected blue to red emission ratios derived from the spectra. The time axis is ms from the lightning/elve associated with the sprite.

Stenbaek-Nielsen et al., 2013). As mentioned above we do not show the data for the beads in the lower panels of Figure 3 since there are essentially no blue emissions detected.

The downward propagating streamer in Figure 3 fades near the bottom of the field of view, but there are no usable spectra covering the fade. However, we do have spectra covering the fade of another downward propagating streamer in the same event. The streamer enters the field of view from above slightly left of the streamer in Figure 3 and 0.1 ms earlier. Data for this streamer are presented in Figure 4 using the same format as for Figure 3. Initially there are significant blue emissions, but toward the end, as the streamer fades, the blue/red ratio decreases to near 0. We see that too in other time series covering streamer fade. We do not plot the estimated error for the last three data points; the streamer is here very faint and error estimation becomes meaningless.

The initial ratios in the streamer are higher than those shown in Figure 3, but this is very likely an artifact of the assumption that all features in the images are at the same range. The streamer initiates in the halo as did the streamer in Figure 3, but it is higher in the Phantom field of view indicating a higher altitude which leads to a smaller quenching correction. A more likely interpretation is that the streamer originates closer to the aircraft and therefore higher in the field of view but not higher in altitude. If we set the range so the onset altitude is the same as used for the streamer in Figure 3, the blue/red ratios will be similar to the values shown in Figure 3.

Our data set has 18 time series of downward propagating streamers with 12 spectral time series covering streamer onset and most, 8 of the 12, have onset against a dark sky. For these streamers, in contrast to the streamer shown in Figure 3, the streamer brightness and downward velocity increases gradually. An example is shown in Figure 5 using the same format as Figure 3. This sprite was observed on 19 August 2009, at 05:37:36 UT west of Oklahoma City. We do not have any indication of the causal lightning strike in the high-speed images (luminosity from the strike or an elve). NLDN does report the strike but only with 100 ms time resolution, so we use the first indication of the downward propagating streamer for timing. The event has no stars present that can be used to estimate the error on and confidence in the derived blue/red ratios, but the instrument settings are similar, and we use the Jupiter spectra used for the event in Figures 3 and 4.

The streamer is initially very faint, and the first two data points are included to illustrate the gradual brightness and velocity increase of the streamer. No blue emissions were detected and because of the low brightness we do not estimate the error. As the streamer brightens the downward velocity increases gradually from 0.5 10^7 m/s at onset to a maximum of 1.5 10^7 m/s. The blue/red ratio is low at onset but increases after four frames. The streamer never becomes very bright, and it exits the imager field of view at 1.3 ms.

The event in Figure 5 also has an example of an upward propagating streamer with usable spectra. This is one of six in the total data set. The sequences of upward streamers generally consist of fewer frames, and the red and blue spectral features used for the analysis are often poorly defined because of the presence of other activity nearby. Essentially, well-defined spectra are recorded only for streamers propagating up above the glow and activity in the onset region as in the example in Figure 1. Our best example is the one shown in Figure 5. At streamer onset and toward the end there is less light detected in the blue. The first detection of the upward streamer is at 0.8 ms, but spectra are only usable from 1.1 ms. There are splits in the streamer, and this example does not end with a diffuse cloud at the top as is most often observed. The maximum upward velocity is 1.7 10^7 m/s slightly higher than the maximum velocity, 1.5 10^7 m/s, in the downward streamer in the figure consistent with earlier analysis results by McHarg et al. (2007), Li and Cummer (2009), and Stenbaek-Nielsen et al. (2013).

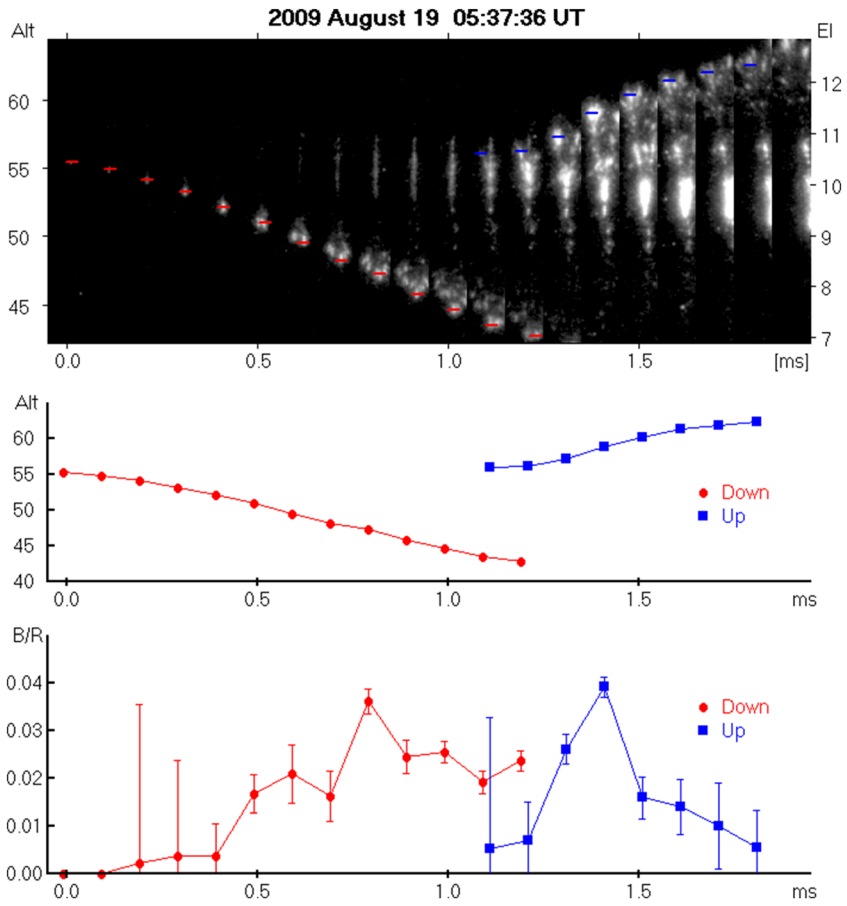

Figure 5. Sprite observed on 2009 August 19 at 05:37:36 UT over western Oklahoma. The top panel has 20 narrow strips extracted from the Phantom images. The image time series shows the development of a downward propagating streamer with onset against a dark sky followed by an upward propagating streamer. The location of the spectra is indicated by red and blue line segments. The center panel has the altitudes of the downward propagating streamer in red and the upward propagating streamer in blue. The bottom panel shows the corresponding blue/red ratios derived from the observed spectra. The data points for the blue/red ratios have been slightly offset to avoid overlapping error bars at 1.1 ms.

5. Discussion

The ratio of the molecular nitrogen emissions in the blue (2PN2) to the red emissions (1PN2) with appropriate corrections for instrument response, quenching, and atmospheric absorption were originally intended to be used to verify sprite model results. Also, it would ideal to be able to separate the blue neutral and ion emissions, but we do not have the spectral resolution for that. However, as discussed in this paper, the assumption of the sprite located at the same range as the causal lightning strike introduces significant uncertainty on the derived altitudes, and therefore on the quenching correction. To illustrate this, we may look at the spectra from the downward and upward propagating streamers shown in the top row of Figure 1. The two spectra are from the same event observed over southern Nebraska on 2 August 2013 at 06:57:20 UT. The observed blue to red ratio for the downward streamer (Figure 1, top left) is 0.36 and 0.13 for the upward streamer (Figure 1, top right). The corresponding altitudes, assuming the same range as the causal lightning strike, are 56.2 and 83.3 km, and correcting for quenching (Figure 2), the ratios become 0.09 and 0.12. This would indicate the upward streamer to be more energetic than the downward streamer, in conflict with modeling by Liu and Pasko (2004). If the range is increased by for example 40 km, the mean distance between the sprite and the causal lightning strike reported by Sao Sabbas et al. (2003), the altitudes for the two features would increase leading to quenching corrected ratios of 0.14 and 0.12; the downward streamer is now the more energetic.

The large uncertainty clearly shows the need for better sprite altitude determination. An obvious solution is to have multiple stations so the sprite altitudes can be derived by triangulation. Another possibility would be to avoid using the red 1PN2 band emissions which are most affected by quenching. Pasko (2007) and Pérez-Invernón et al. (2018) have suggested that 2PN2 and 1NN2+ may be used. However, these optical bands are both in the blue and are difficult to separate in slitless spectroscopic data. Adding a narrow band filtered high-speed imager to augment the spectral images may overcome this problem and would be a good solution for airborne sprite campaigns as reported on here. Observations using multiple imagers with narrow band optical filters were used in some of the early aircraft observations (Armstrong et al., 2000; Morrill et al., 2002) and is used in current observations from the International Space Station (Neubert et al., 2019).

While the blue to red nitrogen emission ratios derived are associated with large uncertainties, we note that just the presence of blue emissions will indicate a more energetic process. The analysis presented here shows that blue emissions are primarily associated with streamer processes early in a sprite event. This supports the suggestion made in the early years of sprite research by Suszcynsky et al. (1998), Armstrong et al. (2000), and later by Pasko (2010) quoting laboratory observations (Ono & Oda, 2005; Simek et al., 1998, 2002; Tochikubo & Teich, 2000) that there are two separate mechanisms associated with the sprite emissions: an initial energetic process, which we here identify as associated with streamer activity, followed by less energetic processes associated with the much longer lasting glow and bead sprite features.

Analysis of the streamer spectra shows temporal changes in the blue to red emissions ratios within individual time series indicating corresponding changes in the energy of the electrons leading to the emissions. The data set has 18 time series of downward propagating streamers with 12 covering streamer onset. Of the 12, 4 have onset in or near a sprite halo and 8 have onset against a dark sky.

The four time series with onset in or near a sprite halo are prompt sprites with streamer onset within a few ms of the causal lightning strike. The streamer brightness and velocity increases very rapidly, and they emerge from the halo with blue to red ratio and downward velocity near the maximum observed for that individual streamer. The maximum downward velocity in the four streamers is in the range 1.5–2.5 10^7 m/s. An example was presented above in Figure 3.

The eight streamers with onset against a dark sky are all delayed sprites with onset 50–300 ms after the lightning strike. In contrast to the rapid brightening and high initial downward velocity observed in the prompt streamers, the brightness and downward velocity increase gradually, typically over about 0.5 ms (five frames). An example was presented in Figure 5 above. Similar examples (but without spectral information) may also be found in Stenbaek-Nielsen et al. (2010). The maximum downward velocity in the eight streamers is in the range 1.0–2.0 10^7 m/s, slightly less than the downward velocity range for the prompt streamers. The delayed sprites appear to have their onset at a lower altitude than the prompt sprites as has been reported by Li et al. (2008) who quote a 5 km altitude difference.

Toward the end of the downward propagation the streamer gradually fades. The streamer fade is covered in 8 of the 18 time series. The fade is often associated with a decrease in downward velocity, but the decrease varies considerably between events and does not appear to be obviously associated with the decrease in streamer brightness. An example was presented in Figure 4. Li and Cummer (2012) found that the streamers begin their significant deceleration where the background field drops below 12–24% of the local electric breakdown field, E_k, and that the fade is at the altitude where the ambient E field is 5% of E_k.

The spectra of the upward propagating streamers appear to follow the same development with little blue emissions at the start and end of the streamers (Figure 5). However, our data set for upward streamers is very limited.

In sprite glow and especially in beads we find little or no blue emissions. Most of the blue emissions in glow are observed early when streamer activity is present. Komuro et al. (2013) reports that laboratory streamers in full pressure air have both “primary” and “secondary” streamers. In these laboratory experiments, primary streamers have higher electron energies and do not last as long as secondary streamers. We speculate that the glows in sprites may be analogous to the secondary streamers reported by Komuro et al. (2013). As seen in Figure 3 the glows last significantly longer than either the downward or upward directed streamers, and have smaller B/R ratios, indicating the possibility of reduced electric field and potentially smaller electron energies.

We do have examples where the blue emissions extend beyond the end of streamer activity, as determined from the high-speed images. This may indicate that the emissions may not be entirely from streamers within the region of the glow, and we suggest that they may be associated with currents in the streamer channels as first proposed by Liu (2010) and later by Luque et al. (2016). Luque et al. (2016) showed that glow and beads in the same streamer channel decay with the same time constant even though they were several scale heights apart in altitude indicating a coupling of the processes within the channel. They suggested a model in which the emissions in the glow and beads are produced by the same process driven by the current in the channel. The local E field in the channel is dictated by the current which, through an electron attachment instability, drives the local plasma in the channel into one of two states: a high conductivity state resulting in a low E field and no optical emissions, or a low conductivity state resulting in a high E field and optical emissions which would be the channel glow and beads. The E field in this model is naturally limited to the local field required for ionization, E_k; if the field locally increases above E_k, ionization would occur increasing the conductivity, and consequently, with the current being constant, the local E field in the channel would decrease. As the sprite decays the current decreases, and the E field would decrease as well. Eventually, there will be only 1P emissions present. As the current decays further there will be no optical emissions, but the channel will remain providing a seed for sprite reignition as is often observed (Sentman et al., 2008; Stenbaek-Nielsen et al., 2000, 2013).

Data Availability Statement

The data presented here are available on Open Science Framework in project "Sprite Spectra at 10,000 fps" (https://osf.io/nmey2/files/). The data are also available from H. Stenbaek-Nielsen (hcnielsen@alaska.edu) or M. G. McHarg (matthew.mcharg@afacademy.af.edu).

Acknowledgments

We gratefully acknowledge the support of the NSF/NCAR High Performance Instrumented Airborne Platform for Environmental Research (HIAPER) project, as well as the pilots and technical staff that made the HIAPER Gulfstream V missions possible. We also acknowledge the contribution by T. Kanmae who did the early analysis of the spectra, and discussions with N. Liu, F. J. Pérez-Invernón, and A. Malagón-Romero. The research has been supported in part by National Science Foundation grants 1104441 to the University of Alaska Fairbanks and 1201683 to the US Air Force Academy. A. Luque was supported by the European Research Council (ERC) under the European Union H2020 programme/ERC grant agreement 681257.

References

Armstrong, R. A., Shorter, J. A., Taylor, M. J., Suszcynsky, D. M., Lyons, W. A., & Jeong, L. S. (1998). Photometric measurements in the SPRITES '95 & '96 campaigns of nitrogen second positive (399.8 nm) and first negative (427.8 nm) emissions. *Journal of Atmospheric and Solar-Terrestrial Physics*, *60*(7–9), 787–799. https://doi.org/10.1016/S1364-6826(98)00026-1

Armstrong, R. A., Suszcynsky, D. M., Lyons, W. A., & Nelson, T. E. (2000). Multi-color photometric measurements of ionization and energies in sprites. *Geophysical Research Letters*, *27*(5), 653–656. https://doi.org/10.1029/1999GL003672

Babaeva, N. Y., & Naidis, G. V. (1997). Dynamics of positive and negative streamers in air in weak uniform electric fields. *IEEE Tranactions of Plasma Science*, *25*(2), 375–379. https://doi.org/10.1109/27.602514

Cartwright, D. C. (1978). Vibrational populations of the excited states of N_2 under auroral conditions. *Journal of Geophysical Research*, *83*(A2), 517–531. https://doi.org/10.1029/JA083iA02p00517

Cornette, W. M., Acharya, P., Robertson, D., & Anderson, G. P. (1995). Moderate spectral atmospheric radiance and transmittance code (MOSART), *Tech. Rep. PL-TR-94-2244*, Philips Lab., Dir. of Geophys., Hanscom AFB, Mass.

Cummer, S. A., Jaugey, N., Li, J., Lyons, W. A., Nelson, T. E., & Gerken, E. A. (2006). Submillisecond imaging of sprite development and structure. *Geophysical Research Letters*, *33*, L04104. https://doi.org/10.1029/2005GL024969

Dilecce, G., Ambrico, P. F., & De Benedictis, S. (2010). On the collision quenching of $N_2 + (B^2\Sigma^+_u, v = 0)$ by N_2 and O_2 and its influence on the measurement of E/N by intensity ratio of nitrogen spectral bands. *Journal of Physics D: Applied Physics*, *43*(19), 195201. https://doi.org/10.1088/0022-3727/43/19/195201

Gallimberti, I., Hepworth, J. K., & Klewe, R. C. (1974). Spectroscopic investigation of impulse corona discharges. *Journal of Physics D: Applied Physics*, *7*(6), 880–898. https://doi.org/10.1088/0022-3727/7/6/315

Gordillo-Vázquez, F. J., Luque, A., & Simek, M. (2012). Near infrared and ultraviolet spectra of TLEs. *Journal of Geophysical Research*, *117*, A05329. https://doi.org/10.1029/2012JA017516

Gordillo-Vázquez, F. J., Passas, M., Luque, A., Sánchez, J., van der Velde, O. A., & Montanyà, J. (2018). High spectral resolution spectroscopy of sprites: A natural probe of the mesosphere. *Journal of Geophysical Research: Atmospheres*, *123*, 2336–2346. https://doi.org/10.1002/2017JD028126

Hampton, D. L., Heavner, M. J., Wescott, E. M., & Sentman, D. D. (1996). Optical spectral characteristics of sprites. *Geophysical Research Letters*, *23*(1), 89–92. https://doi.org/10.1029/95GL03587

Ihaddadene, M. A., & Celestin, S. (2017). Determination of sprite streamers altitude based on N_2 spectroscopic analysis. *Journal of Geophysical Research: Space Physics*, *122*, 1000–1014. https://doi.org/10.1002/2016JA023111

Kanmae, T., Stenbaek-Nielsen, H. C., & McHarg, M. G. (2007). Altitude resolved sprite spectra with 3 ms temporal resolution. *Geophysical Research Letters*, *34*, L07810. https://doi.org/10.1029/2006GL028608

Kanmae, T., Stenbaek-Nielsen, H. C., McHarg, M. G., & Haaland, R. K. (2010a). Observation of sprite streamer head's spectra at 10,000 fps. *Journal of Geophysical Research*, *115*, A00E48. https://doi.org/10.1029/2009JA014546

Kanmae, T., Stenbaek-Nielsen, H. C., McHarg, M. G., & Haaland, R. K. (2010b). Observation of blue sprite spectra at 10,000 fps. *Geophysical Research Letters*, *37*, L13808. https://doi.org/10.1029/2010GL043739

Komuro, A., Ono, R., & Tetsuji Oda, T. (2013). Effects of pulse voltage rise rate on velocity, diameter and radical production of an atmospheric-pressure streamer discharge. *Plasma Sources Science and Technology*, *22*(4), 045002. https://doi.org/10.1088/0963-0252/22/4/045002

Kuo, C.-L., Hsu, R. R., Chen, A. B., Su, H. T., Lee, L. C., Mende, S. B., et al. (2005). Electric fields and electron energies inferred from the ISUAL recorded sprites. *Geophysical Research Letters*, *32*, L19103. https://doi.org/10.1029/2005GL023389

Li, J., & Cummer, S. (2012). Relationship between sprite streamer behavior and lightning-driven electric fields. *Journal of Geophysical Research*, *117*, A01317. https://doi.org/10.1029/2011JA016843

Li, J., & Cummer, S. A. (2009). Measurement of sprite streamer acceleration and deceleration. *Geophysical Research Letters*, *36*, L10812. https://doi.org/10.1029/2009GL037581

Li, J., Cummer, S. A., Lyons, W. A., & Nelson, T. E. (2008). Coordinated analysis of delayed sprites with high-speed images and remote electromagnetic fields. *Journal of Geophysical Research*, *113*, D20206. https://doi.org/10.1029/2008JD010008

Liu, N. Y. (2010). Model of sprite luminous trail caused by increasing streamer current. *Geophysical Research Letters*, *37*, L04102. https://doi.org/10.1029/2009GL042214

Liu, N. Y., & Pasko, V. P. (2004). Effects of photoionization on propagation and branching of positive and negative streamers in sprites. *Journal of Geophysical Research*, *109*, A04301. https://doi.org/10.1029/2003JA010064

Liu, N. Y., Pasko, V. P., Adams, K., Stenbaek-Nielsen, H. C., & McHarg, M. G. (2009). Comparison of acceleration, expansion, & brightness of sprite streamers obtained from modeling and high-speed video observations. *Journal of Geophysical Research*, *114*, A00E03. https://doi.org/10.1029/2008JA013720

Liu, N. Y., Pasko, V. P., Burkhardt, D. H., Frey, H., Mende, S., Su, H.-T., et al. (2006). Comparison of results from sprite streamer modeling with spectrophotometric measurements by ISUAL instrument on FORMOSAT-2 satellite. *Geophysical Research Letters*, *33*, L01101. https://doi.org/10.1029/2005GL024243

Liu, N. Y., Pasko, V. P., Frey, H., Mende, S., Su, H.-T., Chen, A., et al. (2009). Assessment of sprite initiating electric fields and quenching altitude of a1Pg state of N_2 using sprite streamer modeling and ISUAL spectrophotometric measurements. *Journal of Geophysical Research*, *114*, A00E02. https://doi.org/10.1029/2008JA013735

Luque, A., Ratushnaya, V., & Ebert, U. (2008). Positive and negative streamers in ambient air: Modelling evolution and velocities. *Journal of Physics D: Applied Physics*, *41*(23), 234005. https://doi.org/10.1088/0022-3727/41/23/234005

Luque, A., Stenbaek-Nielsen, H. C., McHarg, M. G., & Haaland, R. (2016). Sprite beads and glows arising from the attachment instability in streamer channels. *Journal of Geophysical Research: Space Physics*, *121*, 2431–2449. https://doi.org/10.1002/2015JA022234

Lyons, W. (1996). Sprite observations above the U.S. high plains in relation to their parent thunderstorm systems. *Journal of Geophysical Research*, *101*(D23), 29,641–29,652. https://doi.org/10.1029/96JD01866

McHarg, M. G., Stenbaek-Nielsen, H. C., & Kammae, T. (2007). Observation of streamer formation in sprites. *Geophysical Research Letters*, *34*, L06804. https://doi.org/10.1029/2006GL027854

Mende, S. B., Rairden, R. L., Swenson, G. R., & Lyons, W. A. (1995). Sprite spectra; N_2 1 PG band identification. *Geophysical Research Letters*, *22*(19), 2633–2636. https://doi.org/10.1029/95GL02827

Morrill, J., Bucsela, E., Siefring, C., Heavner, M., Berg, S., Moudry, D., et al. (2002). Electron energy and electric field estimates in sprites derived from ionized and neutral N_2 emissions. *Geophysical Research Letters*, *29*(10), 1462. https://doi.org/10.1029/2001GL014018

Neubert, T., Østgaard, N., Reglero, V., Blanc, E., Chanrion, O., Oxborrow, C. A., et al. (2019). The ASIM mission on the International Space Station. *Space Science Reviews*, *215*(2), 26. https://doi.org/10.1007/s11214-019-0592-z

Ono, R., & Oda, T. (2005). Nitrogen oxide g-band emission from primary and secondary streamers in pulsed positive corona discharge. *Journal of Applied Physics*, *97*(1), 013302. https://doi.org/10.1063/1.1829371

Pasko, V. P. (2007). Red sprite discharges in the atmosphere at high altitude: The molecular physics and the similarity with laboratory discharges. *Plasma Sources Science and Technology*, *16*(1), S13–S29. https://doi.org/10.1088/0963-0252/16/1/S02

Pasko, V. P. (2010). Recent advances in theory of transient luminous events. *Journal of Geophysical Research*, *115*, A00E35. https://doi.org/10.1029/2009JA014860

Pasko, V. P., & Stenbaek-Nielsen, H. C. (2002). Diffuse and streamer regions of sprites. *Geophysical Research Letters*, *29*(10), 1440. https://doi.org/10.1029/2001GL014241

Pérez-Invernón, F. J., Luque, A., Gordillo-Vázquez, F. J., Sato, M., Ushio, T., Adachi, T., & Chen, A. B. (2018). Spectroscopic diagnostic of halos and elves detected from space-based photometers. *Journal of Geophysical Research: Atmospheres*, *123*, 12,917–12,941. https://doi.org/10.1029/2018JD029053

Qin, J., & Pasko, V. P. (2014). On the propagation of streamers in electrical discharges. *Journal of Physics D: Applied Physics*, *47*(43), 435202. https://doi.org/10.1088/0022-3727/47/43/435202

Sao Sabbas, F., Sentman, D., Wescott, E., Pinto, O. Jr., Mendes, O. Jr., & Taylor, M. (2003). Statistical analysis of space-time relationships between sprites and lightning. *Journal of Atmospheric and Solar-Terrestrial Physics*, *65*(5), 525–535. https://doi.org/10.1016/S1364-6826(02)00326-7

Sato, M., Mihara, M., Adachi, T., Ushio, T., Morimoto, T., Kikuchi, M., et al. (2016). Horizontal distributions of sprites derived from the JEM-GLIMS nadir observations. *Journal of Geophysical Research: Atmospheres*, *121*, 3171–3194. https://doi.org/10.1002/2015JD024311

Sentman, D. D., Stenbaek-Nielsen, H. C., McHarg, M. G., & Morrill, J. (2008). Plasma chemistry of sprite streamers. *Journal of Geophysical Research*, *113*, D11112. https://doi.org/10.1029/2007JD008941

Sentman, D. D., Wescott, E. M., Osborne, D. L., Hampton, D. L., & Heavner, M. J. (1995). Preliminary results from the Sprites94 aircraft campaign: 1. Red sprites. *Geophysical Research Letters*, *22*, 1205–1208. https://doi.org/10.1029/95GL00583

Simek, M., Babicky, V., Clupek, M., DeBenedictis, S., Dilecce, G., & Sunka, P. (1998). Excitation of $N_2(C^3\Pi u)$ and $NO(A^2\Sigma^+)$ states in a pulsed positive corona discharge in N_2, N_2-O_2 and N_2-NO mixtures. *Journal of Physics D: Applied Physics*, *35*, 2591–2602.

Simek, M., DeBenedictis, S., Dilecce, G., Babicky, V., Clupek, M., & Sunka, P. (2002). Time and space resolved analysis of $N_2(C^3\Pi u)$ vibrational distributions in pulsed positive corona discharge. *Journal of Physics D: Applied Physics*, *35*(16), 1981–1990. https://doi.org/10.1088/0022-3727/35/16/312

Stanley, M., Krehbiel, P., Brook, M., Moore, C., Rison, W., & Abrahams, B. (1999). High speed video of initial sprite development. *Geophysical Research Letters*, *26*(20), 3201–3204. https://doi.org/10.1039/1999GL010673

Stenbaek-Nielsen, H. C., Haaland, R. K., McHarg, M. G., Hensley, B. A., & Kanmae, T. (2010). Sprite initiation altitude measured by triangulation. *Journal of Geophysical Research*, *115*, A00E12. https://doi.org/10.1029/2009JA014543

Stenbaek-Nielsen, H. C., Kanmae, T., McHarg, M. G., & Haaland, R. (2013). High-speed observations of sprite streamers. *Survey of Geophysics*, *34*(6), 769–795. https://doi.org/10.1007/s10712-013-9224-4

Stenbaek-Nielsen, H. C., & McHarg, M. G. (2008). High time-resolution sprite imaging: Observations and implications. *Journal of Physics D: Applied Physics*, *41*(23), 234009. https://doi.org/10.1088/0022-3727/41/23/234009

Stenbaek-Nielsen, H. C., McHarg, M. G., Kanmae, T., & Sentman, D. D. (2007). Observed emission rates in sprite streamer heads. *Geophysical Research Letters*, *34*, L11105. https://doi.org/10.1029/2007GL029881

Stenbaek-Nielsen, H. C., Moudry, D. R., Wescott, E. M., Sentman, D. D., & Sao Sabbas, F. T. (2000). Sprites and possible mesospheric effects. *Geophysical Research Letters*, *27*(23), 3829–3832. https://doi.org/10.1029/2000GL003827

Suszcynsky, D. M., Roussel-Dupre, R., Lyons, W. A., & Armstrong, R. A. (1998). Blue-light imagery and photometry of sprites. *Journal of Atmospheric and Solar - Terrestrial Physics*, *60*(7–9), 801–809. https://doi.org/10.1016/S1364-6826(98)00027-3

Taylor, J. R. (1997). *An introduction to error analysis*. Sausalito, CA: University Science Books.

Tochikubo, F., & Teich, T. H. (2000). Optical emission from a pulsed corona discharge and its associated reactions, Jpn. *Journal of Physics D: Applied Physics*, *39*, 1343–1350.

Vallance Jones, A. (1974). *Aurora*. Dordrecht, Netherlands: D. Reidel. https://doi.org/10.1007/978-94-010-2099-2

Wescott, E. M., Stenbaek-Nielsen, H. C., Sentman, D. D., Heavner, M. T., Moudry, D. R., & Sao Sabbas, F. T. (2001). Triangulation of sprites, associated halos and their possible relation to causative lightning and micro-meteors. *Journal of Geophysical Research*, *106*(A6), 10,467–10,477. https://doi.org/10.1029/2000JA000182

Yang, J., Lu, G., Lee, L., & Feng, G. (2015). Long-delayed bright dancing sprites with large horizontal displacement from its parent flash. *Journal of Atmospheric and Solar-Terrestrial Physics*, *129*, 1–5. https://doi.org/10.1016/j.jastp.2015.04.001